



Review

Overview of Position-Sensorless Technology for Permanent Magnet Synchronous Motor Systems

Yulei Xu ¹, Ming Yao ^{2,*} and Xiaodong Sun ^{1,*}

¹ Automotive Engineering Research Institute, Jiangsu University, Zhenjiang 212013, China

² School of Automobile and Traffic Engineering, Jiangsu University, Zhenjiang 212013, China

* Correspondence: ymluck@ujs.edu.cn (M.Y.); xdsun@ujs.edu.cn (X.S.); Tel.: +86-0511-8878-2845 (X.S.)

Abstract: In recent years, permanent magnet synchronous motors (PMSMs) have been widely used in industry. Position-sensorless control has the advantages of reducing costs and improving reliability, and is becoming one of the most promising technologies for permanent magnet synchronous motors. This article reviews the main position-sensorless technologies. The advantages and disadvantages of model-based and saliency-based techniques were summarized and compared. Finally, the developmental trends and research directions of position-sensorless technology were discussed.

Keywords: permanent magnet synchronous motor (PMSM); sensorless control; model-based method; saliency-based method

1. Introduction

Due to global warming and the energy crisis, new energy vehicles with fewer emissions, less pollution, and higher energy conversion efficiency are increasingly favored by governments and enterprises worldwide [1–4]. Permanent magnet synchronous motors (PMSMs) have been widely used in the industry due to the advantages of high power density, high efficiency, and a rapid control response [5–11].

A PMSM drive system is a typical nonlinear control system. To obtain good control performance, field-oriented control (FOC) [12–17], direct torque control (DTC) [18–25], sliding mode control (SMO) [26–33], and model predictive control (MPC) [34–44] have been used to improve the control performance of PMSMs. In [21], a novel DTC control strategy was proposed, which used the torque error square minimization technique to determine the duty cycle, thereby reducing the ripple size of the PMSM. As for the design of the observer, the work of [29] studied the main problems and developmental trends of the observer. As an efficient control strategy, MPC is used more and more widely. The authors of [35] proposed a sensorless control MPCC control scheme which enhanced the robustness of the system and improved the accuracy of estimating the rotor's position.

However, these control methods need accurate information on the rotor's position and speed, and the acquisition of the rotor's position signals relies on mechanical sensors. Installing mechanical sensors not only increase the manufacturing costs and complexity of the system but also reduce the operating reliability of the system under extreme conditions. To solve this issue, sensorless control schemes have been invented. Sensorless control technology uses specific algorithms to estimate the rotor's position and speed by detecting relevant signals in the motor's windings. This control scheme has gradually become a trend in the development of PMSM control systems.

Over the past few decades, researchers have developed sensorless control techniques for a wide range of speeds from zero to high speed. Figure 1 shows the classification of sensorless technology approaches. Depending on the operating speed, sensorless control schemes can be divided into two categories: model-based methods [45–111] and saliency-based methods [112–167]. When the motor operates in the medium- to high-speed range, a



Citation: Xu, Y.; Yao, M.; Sun, X. Overview of Position-Sensorless Technology for Permanent Magnet Synchronous Motor Systems. *World Electr. Veh. J.* **2023**, *14*, 212. <https://doi.org/10.3390/wevj14080212>

Academic Editor: C. C. Chan

Received: 5 July 2023

Revised: 4 August 2023

Accepted: 9 August 2023

Published: 10 August 2023



Copyright: © 2023 by the authors. Licensee MDPI, Basel, Switzerland. This article is an open access article distributed under the terms and conditions of the Creative Commons Attribution (CC BY) license (<https://creativecommons.org/licenses/by/4.0/>).

model-based approach is used. These mainly include two schemes: back-EMF estimation and flux linkage estimation. However, when the motor is running at low or zero speeds, due to factors such as modeling uncertainty and the nonlinearity of the inverter, the signal-to-noise ratio of the useful signal is very low and it is difficult to extract, so the model-based method does not work well at low speeds. People usually use the method of high frequency signal injection to obtain information on the rotor's position. High-frequency signals mainly include rotating high-frequency voltage signals and pulsating high-frequency voltage signals.

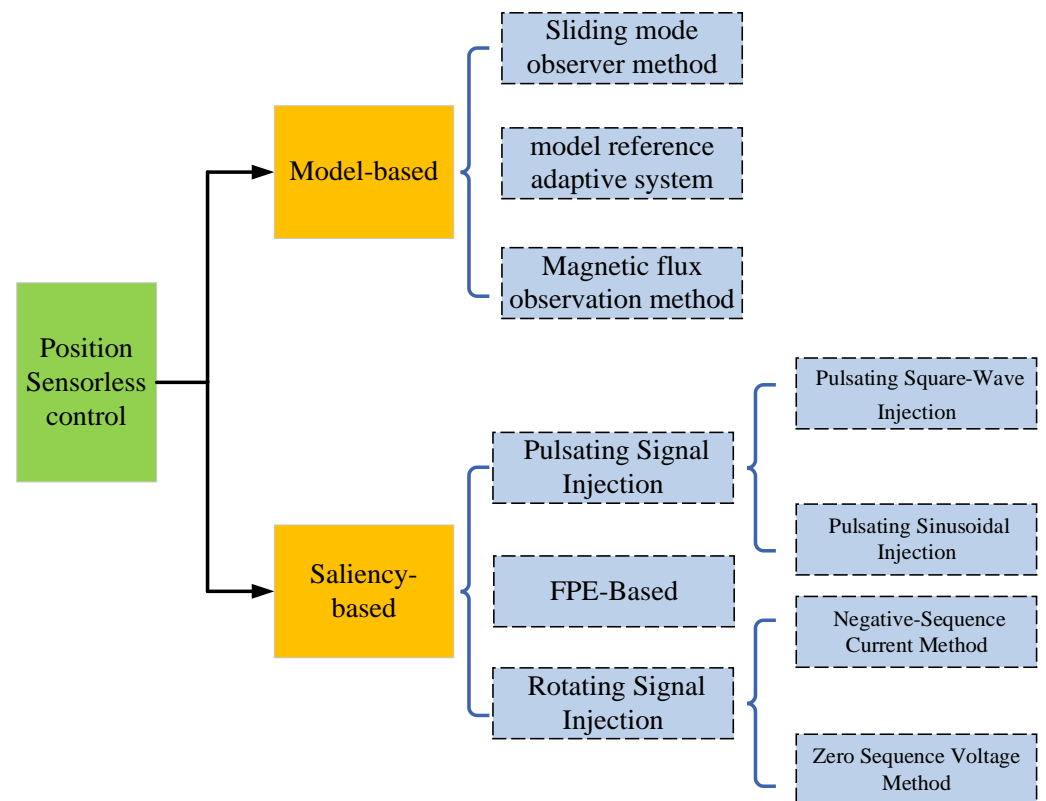


Figure 1. Classification of position-sensorless control methods.

Due to the increasing application of position-sensorless control, this article introduces the most advanced position-sensorless control technologies of permanent magnet synchronous motors from the perspective of technological development. The main contribution is that it summarizes the research status of different methods, as well as the problems and plans for improvement of each method. Essentially, we explored and researched position-sensorless control methods. The feasibility, versatility, and effectiveness of these methods were analyzed and summarized. We also explored the future development and research directions of position-sensorless sensing.

The rest of this article is organized as follows. The Section 2 introduces the drive system of permanent magnet synchronous motors and the basic principles of sensorless control. In the Section 3, various sensorless control methods are introduced. The Section 4 discusses the developmental trends and research direction of position-sensorless sensing. The fifth section is the conclusion of this article.

2. The Composition of PMSM Drive Systems Based on Sensorless Control

2.1. Structure and Mathematical Model of PMSM Systems

Figure 2 shows the structure of a typical PMSM drive system, which mainly includes the current loop and hardware facilities. The hardware facilities include inverter, permanent magnet synchronous motor, power supply and various sensors, while the current loop

is composed of two PI controllers. The operation of the permanent magnet synchronous motor requires an accurate position of the rotor and usually requires position sensors (such as photoelectric encoders and Hall sensors) to obtain accurate information on the rotor’s position, and then accurately control the motion state of the motor. The position-sensorless method can eliminate the position sensor, estimate the rotor’s position and speed through a specific algorithm, and enhance the stability of the system.

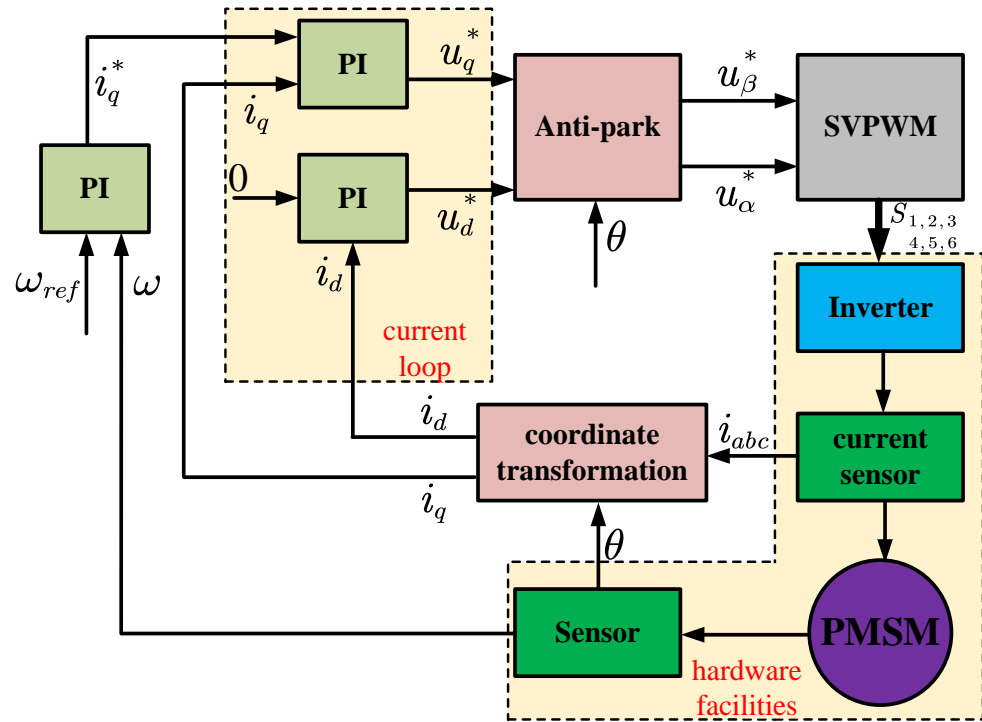


Figure 2. Block diagram of a typical vector control system of a PMSM.

In a typical control block diagram, information on the rotor’s position and speed are obtained by sensors, information on the angle is used for transformation of the coordinates, and information on the speed is used for the speed loop PI controller. The precise operation of the motor is inseparable from accurate information on the rotor’s position and speed.

To better control the operation of the motor, the mathematical model of the permanent magnet synchronous motor can be written as

$$\begin{bmatrix} u_d \\ u_q \end{bmatrix} = R \begin{bmatrix} i_d \\ i_q \end{bmatrix} + \frac{d}{dt} \begin{bmatrix} \psi_d \\ \psi_q \end{bmatrix} + \omega_e \begin{bmatrix} -\psi_q \\ \psi_d \end{bmatrix} \quad (1)$$

where u_d , i_d and ψ_d represent the voltage, current, and magnetic flux on the d-axis, respectively; i_q , u_q and ψ_q represent the current, voltage, and magnetic flux on the q-axis, respectively; ω_e is the electrical angular velocity; and R is the stator resistance. ψ_q and ψ_d can be expressed as

$$\begin{bmatrix} \psi_d \\ \psi_q \end{bmatrix} = \begin{bmatrix} L_d \\ L_q \end{bmatrix} \begin{bmatrix} i_d \\ i_q \end{bmatrix} + \begin{bmatrix} \psi_f \\ 0 \end{bmatrix} \quad (2)$$

where L_d and L_q are the stator inductance of the dq axis, and ψ_f is the permanent magnet flux linkage.

The electromagnetic torque equation of the motor is expressed as shown in Equation (3), and the mechanical equation can be expressed as Equation (4).

$$T_e = \frac{3}{2} p_n i_q [(L_d - L_q) i_d + \psi_f] \quad (3)$$

$$J \frac{d\omega_m}{dt} = T_e - T_L - B\omega_m \quad (4)$$

where p_n is the number of pole pairs, J is the rotational inertia, B is the damping coefficient, ω_m is the mechanical angular velocity, and T_e and T_L are the electromagnetic torque and the load torque, respectively.

It is worth noting that these equations and parameters are significant for sensorless control because information on the rotor's position is included in some parameters.

2.2. Analysis of the Sensorless Control Principle

To achieve a high-performance PMSM control system, it is generally necessary to obtain accurate information on the rotor's position and speed from the position sensor, but when the working conditions of the motor are harsh, the mechanical sensor may cause errors or even damage, and the sensorless control method can avoid the shortcomings of the mechanical sensor. Sensorless control technology detects the electrical signal in the motor's winding and uses the corresponding algorithm to extract the rotor's position and speed.

In the model-based sensorless control methods, the back-EMF or flux linkage contains information on the rotor's position and speed. The following analysis extracts the rotor's position from the back-EMF.

If we rewrite the voltage equation of the PMSM, the voltage equation of the motor in the stationary coordinate system is

$$\begin{bmatrix} u_\alpha \\ u_\beta \end{bmatrix} = \begin{bmatrix} R + pL_d & \omega_e(L_d - L_q) \\ -\omega_e(L_d - L_q) & R + pL_d \end{bmatrix} \begin{bmatrix} i_\alpha \\ i_\beta \end{bmatrix} + \begin{bmatrix} E_\alpha \\ E_\beta \end{bmatrix} \quad (5)$$

where u_α and i_α represent the voltage and current on the α -axis, respectively; u_β and i_β represent the voltage and current on the β -axis, respectively; L_d and L_q are the inductance components of the dq axis; p is the differential operator; and E_α and E_β are the extended back-EMF. E_α and E_β can be expressed as

$$\begin{bmatrix} E_\alpha \\ E_\beta \end{bmatrix} = [(L_d - L_q)(\omega_e i_d - p i_q) + \omega_e \psi_f] \begin{bmatrix} -\sin \theta_e \\ \cos \theta_e \end{bmatrix} \quad (6)$$

where θ_e is the electrical angle.

It can be seen from Equation (6) that the information on the rotor's position θ_e is included in the extended back-EMF. Therefore, only by obtaining the back-EMF accurately can the information on the speed and position of the motor be calculated. In general, to obtain an accurate back-EMF, the sliding mode observer method or the model reference adaptive method can be used. Taking the sliding mode observer as an example, by designing the control law of the sliding mode observer, the error can be zero. At this time, the state variable of the observer reaches the sliding mode's surface. According to the equivalent control principle of sliding mode control, the level of control at this time can be regarded as an equivalent level of control, that is, the estimated back-EMF is equal to the actual back-EMF.

After obtaining the accurate counter electromotive force, the information on the rotor's position, angle, and speed can be obtained after some technical processing. Among these technologies, the arctangent method and the phase-locked loop method are the most mature. Among them, the arctangent method usually requires angle compensation, because the use of a low-pass filter will cause a phase delay, which will directly affect the accuracy of the estimated position of the rotor. Compared with the arctangent method, the phase-locked loop method has no phase delay problem. These two methods can obtain the estimated position angle, and by differentiating the position angle θ_e , the rotor's speed can be obtained. At this time, the information on the rotor's position and the rotational speed of the motor are known quantities, and the motor can realize high-performance control.

However, when the motor is running at zero speed or low speed, the model-based method is not available. To obtain accurate information on the rotor's position at zero speed and low speed, the high-frequency signal injection method is an effective method.

A transformation of Equation (1) into the stationary coordinate system can be expressed as

$$\begin{bmatrix} u_\alpha \\ u_\beta \end{bmatrix} = R \begin{bmatrix} i_\alpha \\ i_\beta \end{bmatrix} + \frac{d}{dt} \begin{bmatrix} \psi_\alpha \\ \psi_\beta \end{bmatrix} \quad (7)$$

$$\begin{bmatrix} \psi_\alpha \\ \psi_\beta \end{bmatrix} = \begin{bmatrix} L + \Delta L \cos 2\theta_e & -\Delta L \sin 2\theta_e \\ -\Delta L \sin 2\theta_e & L - \Delta L \cos 2\theta_e \end{bmatrix} \begin{bmatrix} i_\alpha \\ i_\beta \end{bmatrix} + \psi_f \begin{bmatrix} \cos \theta_e \\ \sin \theta_e \end{bmatrix} \quad (8)$$

where $L = (L_d + L_q)/2$ is the average inductance and $\Delta L = (L_q - L_d)/2$ is half the differential inductance.

We define the inductance matrix $L_{\alpha\beta}$ in the static coordinate system as

$$L_{\alpha\beta} = \begin{bmatrix} L + \Delta L \cos 2\theta_e & -\Delta L \sin 2\theta_e \\ -\Delta L \sin 2\theta_e & L - \Delta L \cos 2\theta_e \end{bmatrix} \quad (9)$$

It can be seen from Equation (9) that the inductance matrix contains the information on the rotor's position θ_e .

According to the different injection reference frames, the current main high-frequency signal injection is divided into the rotation signal and the pulse vibration signal.

The high-frequency signal injection method is very suitable for controlling a low-speed motor because of its simple implementation and does not depend on the internal parameters of the motor. However, in the process of signal processing, the use of LPF will reduce the response bandwidth of the whole system, so that the dynamic performance of the system is insufficient, and the precision of control is not high. In addition, because the signal injection needs to consume part of the DC bus voltage, as the motor's speed increases, its performance will also decrease.

Through a brief introduction and analysis of sensorless technologies, it was found that they have many problems. Through in-depth studies of sensorless technologies, more and more researchers have made contributions to improving the performance of motor drive systems. The latest sensorless control methods are described in detail in the next section.

3. An Overview of the Recent Developments in Sensorless Methods of PMSM

The current sensorless control technologies of PMSM are mainly divided into two categories, namely, model-based methods and saliency-based methods. The former are mainly used in the high-speed range of the motor, while the latter are mainly used in the zero-speed and low-speed ranges. This section presents the latest research results regarding these two methods in detail.

3.1. Model-Based Sensorless Methods

Most of the model-based sensorless control techniques can generally be divided into two steps. The first step is estimating the back-EMF or flux linkage, and the second step is observing the position or velocity. The techniques used for estimating the back electromotive force and flux linkage in the first step are relatively mature and can be divided into open-loop methods and closed-loop methods. In the second step, the law needs to be constructed so that the error is zero. When the estimated error of back-EMF and flux linkage tends to zero, the estimated values of back-EMF and flux linkage are equal to their actual values, and then the position and speed of the motor's rotor can be calculated. To improve the performance of estimation, researchers have invented techniques such as the sliding mode observer (SMO) [26–33,45–52], the model reference adaptive system (MRAS) [53–66], the extended Kalman filter (EKF) [67–85], and the state observer (SO) [100–111]. These techniques are described in detail below.

3.1.1. Sliding Mode Observer

Sliding mode control is a control strategy of variable-structure control systems. The difference between this control strategy and the conventional control strategy is the discontinuity of control, that is, the discrete switch control of the sliding mode observer will cause chattering. To reduce chattering, different improvement schemes have been proposed.

The traditional SMO uses the sign function as the switch function, and some researchers have made modifications to the switch function. For example, the sign function can be replaced by the sigmoid function [48], or the super-twisting function [27,45], and the hyperbolic tangent function [30] can be used instead of the sign function. Experiments have shown that these functions can effectively reduce chattering as the switching functions.

In addition to their contribution to reducing the chattering problem, researchers have also improved the performance of the SMO in other ways. For example, when the motor has been running for a long time, the motor's parameters (the stator's resistance, the stator's inductance, etc.) may change, which will cause a mismatch between the set value and the actual value, affecting the accuracy of the estimation and even affecting the stability of the system. To solve this kind of problem, in [45], a second-order sliding mode observer for estimating the online stator's resistance was proposed. Through estimating the online stator's resistance, the change in resistance due to a change in temperature can be considered, which improves the robustness of the system.

In terms of improving the robustness of the system [27–29,47–50], some have proposed an adaptive algorithm for online adjustment of the sliding mode's coefficients [27]. The proposed adaptive algorithm can reduce the error in estimating the position and improve the estimated accuracy of sensorless technologies. In [29], a novel compound discrete-time sliding mode observer based on the stator's flux state was designed, which could simultaneously estimate the disturbance of the flux parameter, the error in the rotor's position, and the load torque. The influence of the disturbance of the flux linkage parameter on the estimation error was eliminated, and the robustness of the system was greatly improved. In addition, some people have studied the parameter uncertainty of PI control [50] and proposed a model-free speed controller based on a hyperlocal model, which has strong control over the uncertainty of the motor's parameters. A new method was developed in [47] to linearize the nonlinear model of a PMSM near the operating point using DO to estimate the load torque and back-EMF. The operating point was updated using DO, and a state feedback controller (SFC) was designed, similar to the gain-scheduled method. Experiments showed that this method enhanced the robustness and dynamic performance of the system. Figure 3 shows a control block diagram of the method.

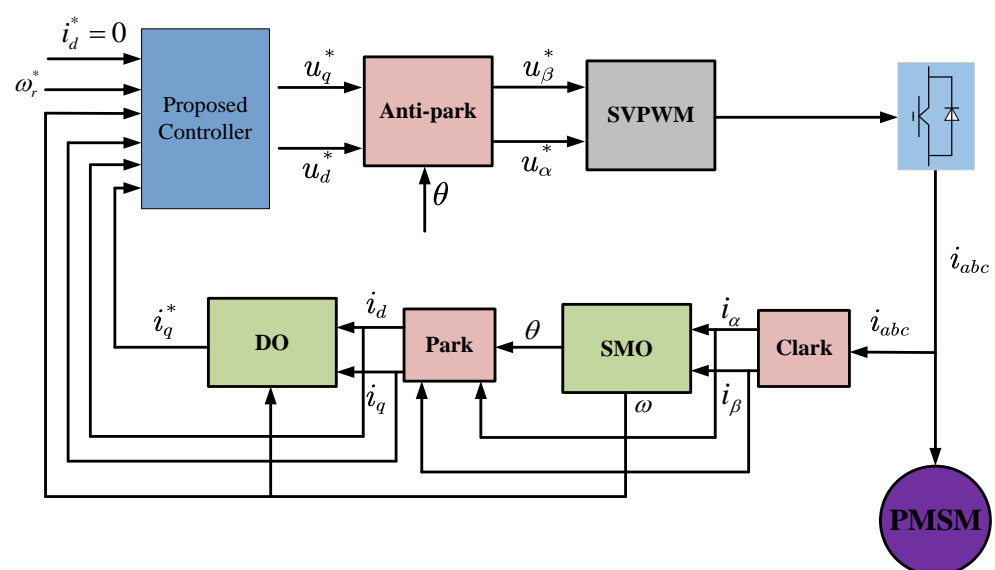


Figure 3. Block diagram of a sensorless control system based on a disturbance observer [47].

3.1.2. Model Reference Adaptive Systems

Model reference adaptive systems (MRAS) are types of adaptive systems. They include three parts, namely, the adjustable model, the reference model, and the adaptive rate. A block diagram of the structure of a MRAS is shown in Figure 4.

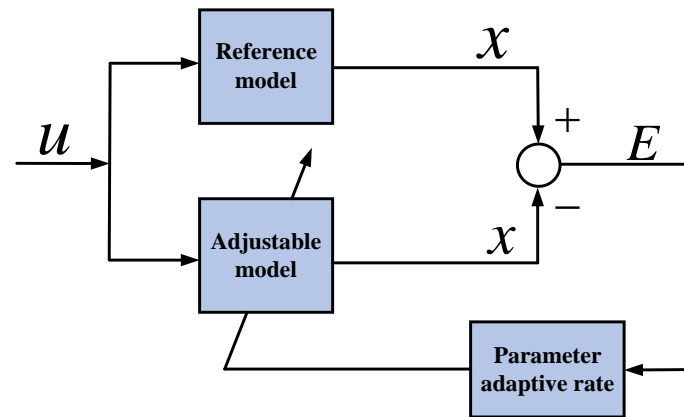


Figure 4. Control block diagram of a model reference adaptive system.

In addition to being used in sensorless control, the model reference adaptive system can also be applied to the identification of parameters to enhance the robustness of the system. In [54], a sensorless control strategy using an MRAS observer was proposed. The proposed MRAS observer could automatically adjust the PI according to the magnitude of the current error variable, and the accuracy of the estimated resistance was greatly improved, which enhanced the robustness of the system. Moreover, the author proposed a voltage compensation method based on a disturbance observer that was, in turn, based on the voltage distortion problem of the voltage source inverter, which improved the performance of the system. The disadvantage was that the system includes two observers, the design is relatively complicated, and the required computing power of the hardware is relatively high. Other researchers have used the MRSA observer to estimate the stator's resistance [55,56]. Regarding the voltage distortion problem of the voltage source inverter [60,62,64,77], ref. [60] proposed a MRAS-based adaptive second-order active flux linkage observer (ASO-AFO) and a MRAS-based VSI nonlinear compensation method. The nonlinearity of the voltage source inverter will lead to harmonic components of the current, which will cause noise, power loss, and additional heating problems. In the study by [60], the root mean square (RMS) value of the cross-product was selected as the objective function, and the voltage was compensated by minimizing the objective function.

In addition to using the MRAS observer alone for estimation of the motor's parameters, some researchers have developed a new method combining artificial intelligence algorithms and MRAS observers [58]. They used the gray wolf algorithm (GWO) to adapt the speed obtained by the MRAS. The proportional–integral (PI) controller parameters of the law were optimized, which enhanced the robustness of the system and improved the accuracy of estimating the rotor's position and speed.

3.1.3. Extended Kalman Filter

The extended Kalman filter is an adaptive system and is also a nonlinear random observer. The parameters or disturbance of the permanent magnet synchronous motor can be estimated online, so the observer's parameters can be adjusted in real time, and the system can be controlled in real time, which improves the performance of the control system.

The EKF can be used for online estimation of the parameters of permanent magnet synchronous motors. The design of the EKF is divided into two steps. The first step is to predict the state vector, and the second step is to correct the predicted state vector. It is worth noting that near zero speed, as the stator's voltage becomes smaller, the state vector's

estimation error will increase, and the system will lose its controlling ability, so the EKF is not available at low speeds.

In addition to using the EKF to estimate the information on the rotor’s position and speed, most people have used the EKF for online parameter estimation [74,75,77,82]. In [77], two EKF-based online parameter identification schemes were proposed, and a general formulation for online parameter estimation was proposed, which can be applied to any electrical parameter. There was an obvious improvement in identifying the stator’s resistance, and it took the influence of noise on the system into account, improving the robustness of the system. Figure 5 shows a structural block diagram of a double extended Kalman filter. In addition to online estimation of the stator’s resistance and inductance, the estimation of the rotor’s flux linkage has also been studied [78]. In addition, some have combined the EKF and adaptive linear active disturbance rejection control [75] to form a degree-of-freedom control strategy, which performed well in terms of dynamic response and antidisturbance performance. However, the shortcomings are also obvious, such as the complex structure, the large amount of calculation, and the relatively expensive cost.

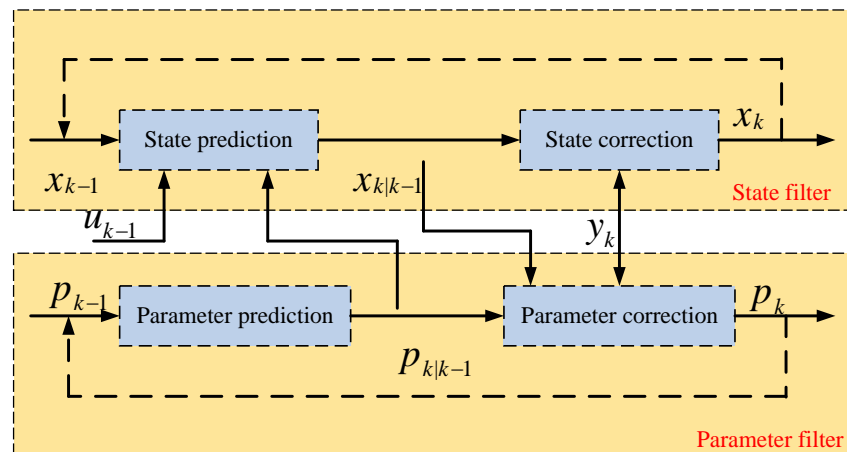


Figure 5. Control block diagram of double extended Kalman filter.

From the content above, we can see that many researchers have used the extended Kalman filter and model reference adaptive systems for online parameter estimation. Table 1 shows a comparison of the online parameter identification methods.

Table 1. Comparison of online parameter identification methods for PMSMs.

Methods	Accuracy	Complexity	Advantage	Disadvantage
MRAS	Medium	Medium	Wide speed range Easy to implement,	Sensitive to noise
RLS	Medium	Medium	the small amount of calculation	Low accuracy
EKF	High	High	Less impact of measurement noise	Complex computation
Neural network	High	High	High accuracy	Complex computation

3.1.4. State Observer

Many scholars have used the state observer (SO) for the sensorless control of the PMSM drive system, mainly to enhance the robustness of the system. The most widely used state observer is the extended state observer (ESO) [102–111]. The ESO is an important part of active disturbance rejection control. It has high precision and is independent of the controlled object model.

The ESO is usually used to estimate the total disturbance [105,108], which generally includes the rotor's flux, load torque, and unmodeled nonlinear disturbances. In [105], the ESO was combined with sliding mode speed control (SMSC), and the control law of SMSC was updated in real time by the estimated total disturbance, which greatly improved the accuracy and robustness to disturbance of the system.

3.2. Saliency-Based Sensorless Methods

The model-based methods above are only suitable for motors running at medium and high speeds. When the motor is running at low speeds, the model-based methods are not available due to the low signal-to-noise ratio. Therefore, in the low-speed range, the sensorless control method should use a significance-based method. The saliency-based methods mainly utilize the position-dependent inductance signal in the stator's winding to realize this, e.g., Equation (9).

The saliency-based methods mainly include two categories. One includes the high-frequency signal (HF) injection methods, and the other includes the fundamental pulsewidth modulation (PWM) excitation (FPE)-based methods. Among them, the high-frequency signal injection method is divided into rotation signal injection and pulse vibration signal injection. These methods are described in detail below.

3.2.1. Rotating Signal Injection

The injected high-frequency voltage signal can be expressed as

$$U_{in} = \begin{bmatrix} u_{\alpha h} \\ u_{\beta h} \end{bmatrix} = U_{in} \begin{bmatrix} \cos(\omega_h t) \\ \sin(\omega_h t) \end{bmatrix} \quad (10)$$

where ω_h is the frequency of the injected high-frequency signal and U_{in} is the amplitude of the high-frequency signal.

After injecting a high-frequency voltage signal, the corresponding equation of the current is

$$\begin{bmatrix} i_{\alpha h} \\ i_{\beta h} \end{bmatrix} = \begin{bmatrix} I_{sp} \sin(\omega_h t) + I_{sn} \sin(-\omega_h t + 2\theta_e) \\ -I_{sp} \cos(\omega_h t) - I_{sn} \cos(-\omega_h t + 2\theta_e) \end{bmatrix} \quad (11)$$

where I_{sp} and I_{sn} are the positive and negative terms of the high-frequency response current, respectively.

Formula (11) can be transformed to the stationary coordinate system as follows:

$$\begin{bmatrix} i_{dh} \\ i_{qh} \end{bmatrix} = \begin{bmatrix} I_{sp} \sin(2\omega_h t) + I_{sn} \sin(2\theta_e) \\ -I_{sp} \cos(2\omega_h t) - I_{sn} \cos(2\theta_e) \end{bmatrix} \quad (12)$$

After obtaining Formula (12), only a low-pass filter is needed to extract the information on the rotor's position.

Figure 6 is a basic block diagram of the rotating high-frequency signal injection method. There are two typical methods based on rotating high-frequency signal injection, namely, the negative-sequence current method [118–124] and the zero-sequence voltage method [125–127]. Both methods are described below.

The phase of the negative-phase-sequence's high-frequency current component contains information on the rotor's position, but to obtain accurate information on the rotor's position, signals such as low-order harmonic currents and the positive-phase-sequence's high-frequency currents must be filtered out. The band-pass filter can remove harmonic currents, and the synchronous shafting high-pass filter can remove the positive-phase-sequence's high-frequency current. A new method of extracting the rotor's position was proposed in [118], which extracts the information on the rotor's position from the relationship between the injected voltage and the induced current, and can also be calculated by using the induced current envelope using an all-pass filter. In this method, there is no time delay and the dynamic performance is improved.

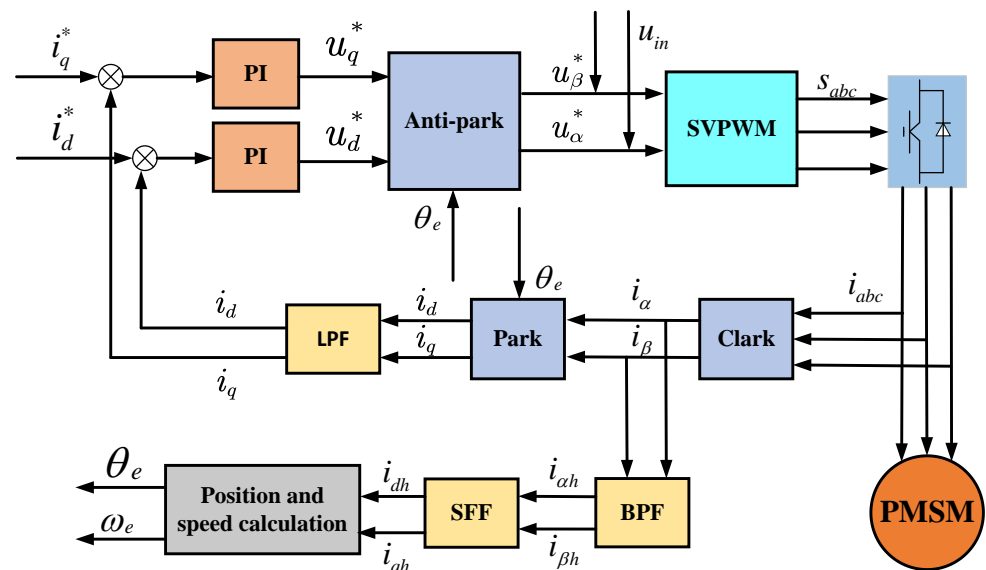


Figure 6. Block diagram of rotating signal injection.

The zero-sequence voltage method was used in [126] for sensorless control of a PMSM. Unlike the conventional high-frequency injection method, the proposed method works on an estimated reference frame with twice the estimated electrical angular velocity of the rotor during anticlockwise rotation. This method is more robust in terms of signal demodulation and produces a carrier response amplitude that is independent of the injection frequency.

3.2.2. Pulsating Signal Injection

The pulsating signal injection method is another effective saliency-based sensorless control scheme. According to the different injected signals, these methods can be divided into two categories: pulsating sinusoidal injection [128–135] and pulsating square wave injection [143–156].

Unlike the rotating HF voltage injection method, the pulsating HF voltage injection method can only inject HF signals on the d-axis of the estimated synchronous rotating coordinate system. To estimate the rotor’s position accurately, an estimated synchronous rotation coordinate system of the rotor is established.

Similar to the rotation signal, the injected pulsating high-frequency signal can be expressed as

$$U_{in} = \begin{bmatrix} u_{dh} \\ u_{qh} \end{bmatrix} = U_{in} \begin{bmatrix} \sin(\omega_h t) \\ 0 \end{bmatrix} \tag{13}$$

where U_{in} is the amplitude of the HF signal, and the symbol “~” indicates the components of the estimated rotor’s frame of reference.

The response current equation is

$$\begin{bmatrix} i_{\alpha h} \\ i_{\beta h} \end{bmatrix} = \begin{bmatrix} \frac{\cos(\theta_e)\cos(\Delta\theta_e)}{L_d} + \frac{\sin(\theta_e)\sin(\Delta\theta_e)}{L_q} \\ \frac{\sin(\theta_e)\cos(\Delta\theta_e)}{L_d} - \frac{\cos(\theta_e)\sin(\Delta\theta_e)}{L_q} \end{bmatrix} \int U_{in} dt \tag{14}$$

where $\Delta\theta_e = \theta_e - \hat{\theta}_e$ is the position’s error. When the position’s error tends to zero, Equation (14) can be written as

$$\begin{bmatrix} i_{\alpha h} \\ i_{\beta h} \end{bmatrix} = \frac{1}{L_d} \begin{bmatrix} \cos(\theta_e) \\ \sin(\theta_e) \end{bmatrix} \cdot \int U_{in} dt. \tag{15}$$

After obtaining Formula (15), the information on the position can be obtained after demodulation of the signal.

Figure 7 is a block diagram of heartbeat signal injection.

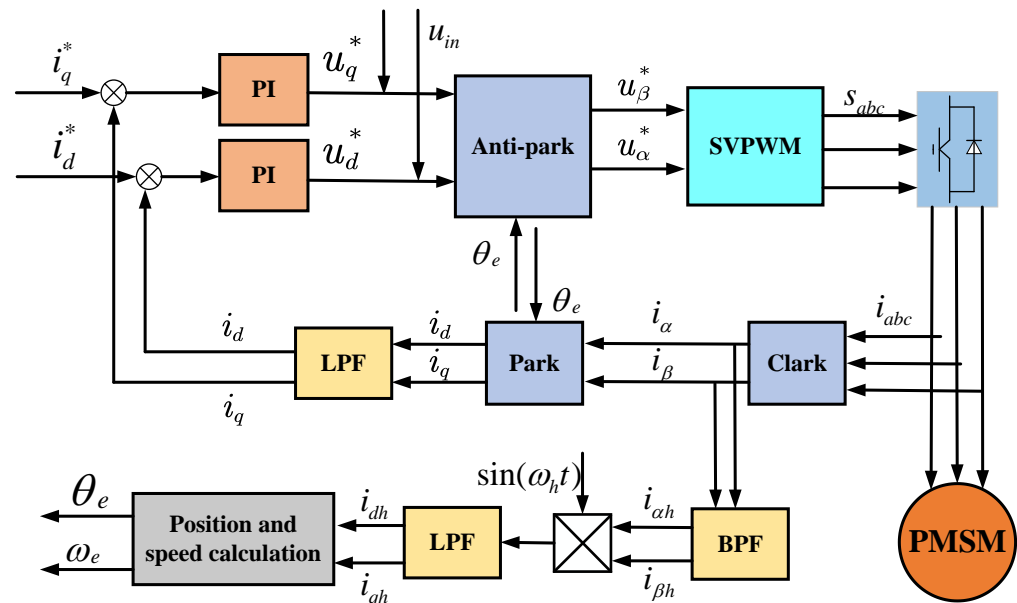


Figure 7. Block diagram of pulsating signal injection.

To improve the accuracy, some researchers injected two kinds of HF pulsation signals with different frequencies [135]. In [131], the author proposed a new pulsating sinusoidal signal injection method, using three HF pulsation signals with different frequencies and amplitudes. The voltage is injected into the ABC frame. This method demodulates the three frequency components in the response current signal and then combines them together to directly calculate the rotor's position, which reduces the influence of the system's delay and improves the accuracy of the estimation.

Compared with the pulsating sinusoidal signal, the pulsating square wave signal has a high injection frequency, which is beneficial for the separation and extraction of high-frequency signals. The square-wave injection voltage at different frequencies was evaluated in [93], and the results showed that designing an appropriate frequency of the injection voltage could significantly improve the performance of the system. Some researchers also proposed an improved HF square wave voltage injection method, which is more robust to voltage errors [156].

In practical applications, researchers have also considered the inverter's dead zone [145], cross-saturation [131,132,147,152], the second harmonic [134,138], and variations in the machine's parameters [135–137,140,146] to improve the accuracy of estimation.

3.2.3. FPE-Based Methods

In addition to injecting high-frequency signals, the abovementioned high-frequency signal injection methods also require an observer to process the signals to obtain the accurate position of the rotor, which increases the complexity and cost of the system. To solve this problem, a control method based on FPE has been proposed.

FPE-based methods can be mainly divided into three categories, namely indirect flux detection by in-line reactance measurement (INFORM) [158–160], the zero-sequence current derivative (ZSCD) measurement method [161–163], and the zero-voltage vector injection method (ZVVI) [164–167].

INFORM works by applying a voltage vector in different directions and then measuring the resulting response current. The authors of [159] improved INFORM to reduce the current's harmonics and switching losses. The working principle of ZSCD is as follows. The test signal is injected into the system, the zero-sequence current derivative of the inductor can be obtained, and the information on the rotor's position and speed

can be obtained. The ZSCD method is simple and has excellent performance, but it needs to be connected to the neutral point, which limits the development of the ZSCD. ZVVI combines the derived calculations of the current and zero-voltage vector injection, which is effective for sensorless control of a PMSM during zero-speed and low-speed operation. These control methods are worthy of further study.

To compare the differences of several methods more intuitively, Table 2 gives the advantages and disadvantages of various methods.

Table 2. Comparison of Saliency-Based Methods.

Method	Advantages	Disadvantages
Rotating signal injection	Does not require information on the initial location, good robustness	Only applicable to salient pole motors
Pulsating sinusoidal injection	Low injection frequency. The influence of the inverter's nonlinearity is small.	LPF affects the system's bandwidth and has insufficient dynamic performance
Pulsating square wave injection	High injection frequency. High-frequency signal extraction is simple, and the influence of the inverter's nonlinearity is small	LPF affects the system's bandwidth and has insufficient dynamic performance. It needs information on the initial location
FPE-based methods	No external signal injection required, no high-frequency noise	High requirements of the current signal sampling circuit

In this section, the high-speed sensorless control methods and the low-speed sensorless control methods are summarized. They all have their own advantages and disadvantages, and some shortcomings still need to be overcome. Table 3 [123,168–189] presents the characteristics of various methods.

Table 3. Comparison of various sensorless methods.

Categories	Speed Range	Advantages	Disadvantages
SMO	Medium and high speed	Good robustness	Chattering exists. Heavy calculation demands
MRAS	Medium and high speed	Simple structure, easy to implement quick response	Depends on the motor's parameters
EKF	Medium and high speed	Strong anti-interference resistance to noise	Heavy calculation
SO	Medium and high speed	Good robustness	Complex structure
Rotating signal injection	Startup and low speed	Easy to implement, good robustness	High-frequency noise, torque ripple
Pulsating signal injection	Startup and low speed	Suitable for salient pole and hidden pole motors	LPF affects the system's bandwidth
FPE-based methods	Startup and low-speed	No need to inject a signal	High requirements for the hardware detection circuit

4. Future Directions

According to the summary and review of the existing methods, sensorless control methods have been developed rapidly. However, with the increasing application of sensorless control systems and the increasingly complex working environment, sensorless control must adapt to more scenarios. Some development trends mainly focus on the following aspects.

4.1. High Dynamic Performance throughout the Full Speed Range

The dynamic performance of a PMSM directly affects the quality of the motor. A good motor drive system must have good dynamic performance. In the future, dy-

dynamic performance will attract more and more attention to adapt to high-performance application scenarios.

4.2. Smooth Switching between Low Speed and High Speed

At present, there is no mature and reliable solution that can efficiently and stably realize the position-sensorless control of permanent magnet synchronous motors across the full speed range. Traditional position-sensorless control techniques are mainly divided into two categories, namely high-speed model-based methods and low-speed saliency-based methods, which lead to changes in the control methods when transitioning from low speeds to medium and high speeds. A combination of these two methods constitutes a hybrid control strategy [190–192], but the difficulty of the hybrid control strategy is how to switch between the two methods without large fluctuations in speed. Therefore, how to smoothly switch from low speeds to high speeds is a direction worth studying.

4.3. Sensorless Control of Ultra-High-Speed PMSMs

In some specific occasions, permanent magnet synchronous motors may require ultra-high speed, such as centrifugal compressors, turbo generators, etc. When the motor is running at ultra-high speed (e.g., 15,000 rpm), the mechanical position sensor is not reliable; to solve this problem, sensorless control of the motor is required [193–195]. Moreover, the stability of the PMSM is an important challenge when the motor operates at ultra-high speeds. Therefore, it is necessary to study the stable control methods of permanent magnet synchronous motors at ultra-high speed.

4.4. High Robustness under Heavy and Changing Loads

As we all know, drastic changes in the load will cause fluctuations in speed, so how to reduce such fluctuations is the focus of research. Strong robustness to load disturbance is an important indicator for evaluating the performance of sensorless control, and how to maintain accurate information on the rotor's position when the load changes drastically is an important research direction.

4.5. High Robustness to Changes in the Motor's Parameters

As the operation or working conditions of the motor change, the mechanical parameters of the motor (such as the stator's resistance, inductance, and flux linkage, etc.) will change, which will lead to a decrease in the performance of control and an increase in the error of estimation. Therefore, to improve the performance of sensorless control, high robustness to variation in the motor's parameters is essential.

5. Conclusions

This article summarized the research status of sensorless control technology used for permanent magnet synchronous motors, and introduces the basic principles of sensorless control. In the high-speed range, the methods of the sliding mode observer, model reference adaptive system, and the Kalman filter have been introduced and compared. In the low-speed range, the methods of rotating high frequency signal injection and pulsating high frequency signal injection have been introduced. However, the methods above still have some limitations, such as sensorless control methods for the full speed domain, etc. To solve these problems, some advanced control theories have been proposed, such as particle swarm optimization algorithms and neural networks. With the development of science and technology, ultra-high-speed sensorless control and high robustness to disturbance will become the focus of research.

Author Contributions: Writing—original draft preparation, Y.X.; supervision, M.Y. and X.S. All authors have read and agreed to the published version of the manuscript.

Funding: This research received no external funding.

Data Availability Statement: No new data were created or analyzed in this study. Data sharing is not applicable to this article.

Conflicts of Interest: The authors declare no conflict of interest.

References

1. Tian, X.; He, R.; Sun, X.; Cai, Y.; Xu, Y. An ANFIS-based ECMS for energy optimization of parallel hybrid electric bus. *IEEE Trans. Veh. Technol.* **2020**, *69*, 1473–1483. [[CrossRef](#)]
2. Sun, X.; Jin, Z.; Xue, M.; Tian, X. Adaptive ECMS with gear shift control by grey wolf optimization algorithm and neural network for plug-in hybrid electric buses. *IEEE Trans. Ind. Electron.* **2023**, *71*, 667–677. [[CrossRef](#)]
3. Sun, X.; Xue, M.; Cai, Y.; Tian, X.; Jin, Z.; Chen, L. Adaptive ECMS based on EF optimization by model predictive control for plug-in hybrid electric buses. *IEEE Trans. Transp. Electrification* **2023**, *9*, 2153–2163. [[CrossRef](#)]
4. Choi, K.; Kim, Y.; Kim, S.-K.; Kim, K.-S. Current and position sensor fault diagnosis algorithm for PMSM drives based on robust state observer. *IEEE Trans. Ind. Electron.* **2021**, *68*, 5227–5236. [[CrossRef](#)]
5. Sun, X.; Cai, F.; Yang, Z.; Tian, X. Finite position control of interior permanent magnet synchronous motors at low speed. *IEEE Trans. Power Electron.* **2022**, *37*, 7729–7738. [[CrossRef](#)]
6. Novak, Z.; Novak, M. Adaptive PLL-based sensorless control for improved dynamics of high-speed PMSM. *IEEE Trans. Power Electron.* **2022**, *37*, 10154–10165. [[CrossRef](#)]
7. Sun, X.; Hu, C.; Lei, G.; Guo, Y.; Zhu, J. State feedback control for a PM hub motor based on gray wolf optimization algorithm. *IEEE Trans. Power Electron.* **2020**, *35*, 1136–1146. [[CrossRef](#)]
8. Yeam, T.-I.; Lee, D.-C. Design of sliding-mode speed controller with active damping control for single-inverter dual-PMSM drive systems. *IEEE Trans. Power Electron.* **2021**, *36*, 5794–5801. [[CrossRef](#)]
9. Li, T.; Sun, X.; Yao, M.; Guo, D.; Sun, Y. Improved finite control set model predictive current control for permanent magnet synchronous motor with sliding mode observer. *IEEE Trans. Transp. Electrification* **2023**. [[CrossRef](#)]
10. Woldegiorgis, A.T.; Ge, X.; Wang, H.; Zuo, Y. An active flux estimation in the estimated reference frame for sensorless control of IPMSM. *IEEE Trans. Power Electron.* **2022**, *37*, 9047–9060. [[CrossRef](#)]
11. Chen, L.; Xu, H.; Sun, X. A Novel Strategy of Control Performance Improvement for Six-Phase Permanent Magnet Synchronous Hub Motor Drives of EVs Under New European Driving Cycle. *IEEE Trans. Veh. Technol.* **2021**, *70*, 5628–5637. [[CrossRef](#)]
12. Lara, J.; Xu, J.; Chandra, A. Effects of Rotor Position Error in the Performance of Field-Oriented-Controlled PMSM Drives for Electric Vehicle Traction Applications. *IEEE Trans. Power Electron.* **2016**, *63*, 4738–4751. [[CrossRef](#)]
13. Candelo-Zuluaga, C.; Riba, J.-R.; Garcia, A. PMSM Parameter Estimation for Sensorless FOC Based on Differential Power Factor. *IEEE Trans. Instrum. Meas.* **2021**, *70*, 1504212. [[CrossRef](#)]
14. Sun, X.; Xiong, Y.; Yao, M.; Tang, X.; Tian, X. A unified control method combined with improved TSF and LADRC for SRMs using modified grey wolf optimization algorithm. *ISA Trans.* **2022**, *131*, 662–671. [[CrossRef](#)] [[PubMed](#)]
15. Kuruppu, S.S.; Abeyratne, S.G. Disambiguation of Uniform Demagnetization Fault From Position Sensor Fault in FOC PMSM Applications. *IEEE Access* **2022**, *10*, 103099–103110. [[CrossRef](#)]
16. Wu, Z.; Yang, Z.; Ding, K.; He, G. Transfer Mechanism Analysis of Injected Voltage Harmonic and its Effect on Current Harmonic Regulation in FOC PMSM. *IEEE Trans. Power Electron.* **2022**, *37*, 820–829. [[CrossRef](#)]
17. Sun, X.; Xu, N.; Yao, M.; Cai, F.; Wu, M. Efficient feedback linearization control for an IPMSM of EVs based on improved firefly algorithm. *ISA Trans.* **2023**, *134*, 431–441. [[CrossRef](#)]
18. Petkar, S.G.; Thippiripati, V.K. A Novel Duty-Controlled DTC of a Surface PMSM Drive With Reduced Torque and Flux Ripples. *IEEE Trans. Ind. Electron.* **2023**, *70*, 3373–3383. [[CrossRef](#)]
19. Sun, X.; Feng, L.; Zhu, Z.; Lei, G.; Diao, K.; Guo, Y.; Zhu, J. Optimal design of terminal sliding mode controller for direct torque control of SRMs. *IEEE Trans. Transp. Electrification* **2022**, *8*, 1445–1453.
20. Wang, M.; Sun, D.; Zheng, Z.; Nian, H. A Novel Lookup Table Based Direct Torque Control for OW-PMSM Drives. *IEEE Trans. Ind. Electron.* **2021**, *68*, 10316–10320. [[CrossRef](#)]
21. Lemma, B.D.; Pradabane, S. Control of PMSM Drive Using Lookup Table Based Compensated Duty Ratio Optimized Direct Torque Control (DTC). *IEEE Access* **2023**, *11*, 19863–19875. [[CrossRef](#)]
22. Nasr, A.; Gu, C.; Wang, X.; Buticchi, G.; Bozhko, S.; Gerada, C. Torque-Performance Improvement for Direct Torque-Controlled PMSM Drives Based on Duty-Ratio Regulation. *IEEE Trans. Power Electron.* **2022**, *37*, 749–760. [[CrossRef](#)]
23. Sun, X.; Xiong, Y.; Yang, J.; Tian, X. Torque ripple reduction for a 12/8 switched reluctance motor based on a novel sliding mode control strategy. *IEEE Trans. Transp. Electrification* **2023**, *9*, 359–369. [[CrossRef](#)]
24. Sun, D.; Chen, W.; Cheng, Y.; Nian, H. Improved Direct Torque Control for Open-Winding PMSM System Considering Zero-Sequence Current Suppression With Low Switching Frequency. *IEEE Trans. Power Electron.* **2021**, *36*, 4440–4451. [[CrossRef](#)]
25. Feng, L.; Sun, X.; Tian, X.; Diao, K. Direct torque control with variable flux for an SRM based on hybrid optimization algorithm. *IEEE Trans. Power Electron.* **2022**, *37*, 6688–6697. [[CrossRef](#)]
26. Ding, L.; Li, Y.W.; Zargari, N.R. Discrete-Time SMO Sensorless Control of Current Source Converter-Fed PMSM Drives With Low Switching Frequency. *IEEE Trans. Ind. Electron.* **2021**, *68*, 2120–2129. [[CrossRef](#)]

27. Sun, X.; Zhu, Y.; Cai, Y.; Yao, M.; Sun, Y.; Lei, G. Optimized-sector-based model predictive torque control with sliding mode controller for switched reluctance motor. *IEEE Trans. Energy Convers.* **2023**. [[CrossRef](#)]
28. Zhao, K.; Yin, T.; Zhang, C.; He, J.; Li, X.; Chen, Y.; Zhou, R.; Leng, A. Robust Model-Free Nonsingular Terminal Sliding Mode Control for PMSM Demagnetization Fault. *IEEE Access* **2019**, *7*, 15737–15748. [[CrossRef](#)]
29. Filho, C.J.V.; Xiao, D.; Vieira, R.P.; Emadi, A. Observers for High-Speed Sensorless PMSM Drives: Design Methods, Tuning Challenges and Future Trends. *IEEE Access* **2021**, *9*, 56397–56415. [[CrossRef](#)]
30. Gong, C.; Hu, Y.; Gao, J.; Wang, Y.; Yan, L. An Improved Delay-Suppressed Sliding-Mode Observer for Sensorless Vector-Controlled PMSM. *IEEE Trans. Ind. Electron.* **2020**, *67*, 5913–5923. [[CrossRef](#)]
31. Yu, K.; Wang, Z. Improved Deadbeat Predictive Current Control of Dual Three-Phase Variable-Flux PMSM Drives With Composite Disturbance Observer. *IEEE Trans. Power Electron.* **2022**, *37*, 8310–8321. [[CrossRef](#)]
32. Kim, H.; Son, J.; Lee, J. A High-Speed Sliding-Mode Observer for the Sensorless Speed Control of a PMSM. *IEEE Trans. Ind. Electron.* **2011**, *58*, 4069–4077.
33. Feng, L.; Sun, X.; Guo, D.; Yao, M.; Diao, K. Advanced torque sharing function strategy with sliding mode control for switched reluctance motors. *IEEE Trans. Transp. Electrif.* **2023**. [[CrossRef](#)]
34. Abu-Ali, M.; Berkel, F.; Manderla, M.; Reimann, S.; Kennel, R.; Abdelrahem, M. Deep Learning-Based Long-Horizon MPC: Robust, High Performing, and Computationally Efficient Control for PMSM Drives. *IEEE Trans. Power Electron.* **2022**, *37*, 12486–12501. [[CrossRef](#)]
35. Sun, X.; Li, T.; Zhu, Z.; Lei, G.; Guo, Y.; Zhu, J. Speed Sensorless Model Predictive Current Control Based on Finite Position Set for PMSM Drives. *IEEE Trans. Transp. Electrif.* **2021**, *7*, 2743–2752. [[CrossRef](#)]
36. Wu, M.; Sun, X.; Zhu, J.; Lei, G.; Guo, Y. Improved Model Predictive Torque Control for PMSM Drives Based on Duty Cycle Optimization. *IEEE Trans. Magn.* **2021**, *57*, 8200505. [[CrossRef](#)]
37. Xu, S.; Sun, Z.; Yao, C.; Zhang, H.; Hua, W.; Ma, G. Model Predictive Control With Constant Switching Frequency for Three-Level T-Type Inverter-Fed PMSM Drives. *IEEE Trans. Ind. Electron.* **2022**, *69*, 8839–8850. [[CrossRef](#)]
38. Xue, C.; Zhou, D.; Li, Y. Finite-Control-Set Model Predictive Control for Three-Level NPC Inverter-Fed PMSM Drives With LC Filter. *IEEE Trans. Ind. Electron.* **2021**, *68*, 11980–11991. [[CrossRef](#)]
39. Tian, X.; Cai, Y.; Sun, X.; Zhu, Z.; Xu, Y. A novel energy management strategy for plug-in hybrid electric buses based on model predictive control and estimation of distribution algorithm. *IEEE/ASME Trans. Mechatron.* **2022**, *27*, 4350–4361. [[CrossRef](#)]
40. Zhang, X.; Bai, H.; Cheng, M. Improved Model Predictive Current Control With Series Structure for PMSM Drives. *IEEE Trans. Ind. Electron.* **2022**, *69*, 12437–12446. [[CrossRef](#)]
41. Xu, T.; Wang, X.; Xiao, D.; Meng, X.; Mao, Y.; Wang, Z. A Novel Two-Mode Inverter-Based Open-Winding PMSM Drive and Its Modulation Strategies. *IEEE Trans. Power Electron.* **2023**, *38*, 8762–8774. [[CrossRef](#)]
42. Chen, L.; Xu, H.; Sun, X.; Cai, Y. Three-Vector-Based Model Predictive Torque Control for a Permanent Magnet Synchronous Motor of EVs. *IEEE Trans. Transp. Electrif.* **2021**, *7*, 1454–1465. [[CrossRef](#)]
43. Luo, Y.; Yang, K.; Zheng, Y. Luenberger Observer-Based Model Predictive Control for Six-Phase PMSM Motor With Localization Error Compensation. *IEEE Trans. Ind. Electron.* **2023**, *70*, 10800–10810. [[CrossRef](#)]
44. Sun, X.; Li, T.; Tian, X.; Zhu, J.G. Fault-tolerant operation of a six-phase permanent magnet synchronous hub motor based on model predictive current control with virtual voltage vectors. *IEEE Trans. Energy Convers.* **2022**, *37*, 337–346. [[CrossRef](#)]
45. Liang, D.; Li, J.; Qu, R. Sensorless Control of Permanent Magnet Synchronous Machine Based on Second-Order Sliding-Mode Observer With Online Resistance Estimation. *IEEE Trans. Ind. Appl.* **2017**, *53*, 3672–3682. [[CrossRef](#)]
46. Sun, X.; Cao, J.; Lei, G.; Guo, Y.; Zhu, J. A robust deadbeat predictive controller with delay compensation based on composite sliding mode observer for PMSMs. *IEEE Trans. Power Electron.* **2021**, *36*, 10742–10752. [[CrossRef](#)]
47. Apte, A.; Joshi, V.A.; Mehta, H.; Walambe, R. Disturbance-Observer-Based Sensorless Control of PMSM Using Integral State Feedback Controller. *IEEE Trans. Power Electron.* **2020**, *35*, 6082–6090. [[CrossRef](#)]
48. Qiao, Z.; Shi, T.; Wang, Y.; Yan, Y.; Xia, C.; He, X. New Sliding-Mode Observer for Position Sensorless Control of Permanent-Magnet Synchronous Motor. *IEEE Trans. Ind. Electron.* **2013**, *60*, 710–719. [[CrossRef](#)]
49. Wang, G.; Hao, X.; Zhao, N.; Zhang, G.; Xu, D. Current Sensor Fault-Tolerant Control Strategy for Encoderless PMSM Drives Based on Single Sliding Mode Observer. *IEEE Trans. Transp. Electrif.* **2020**, *6*, 679–689. [[CrossRef](#)]
50. Li, Z.; Zhang, Z.; Feng, S.; Wang, J.; Guo, X.; Sun, H. Design of Model-Free Speed Regulation System for Permanent Magnet Synchronous Linear Motor Based on Adaptive Observer. *IEEE Access* **2022**, *10*, 68545–68556. [[CrossRef](#)]
51. Sun, X.; Hu, C.; Zhu, J.; Wang, S.; Zhou, W.; Yang, Z.; Lei, G.; Li, K.; Zhu, B.; Guo, Y. MPTC for PMSMs of EVs with multi-motor driven system considering optimal energy allocation. *IEEE Trans. Magn.* **2019**, *55*, 1–6. [[CrossRef](#)]
52. Zuo, Y.; Lai, C.; Iyer, K.L.V. A Review of Sliding Mode Observer Based Sensorless Control Methods for PMSM Drive. *IEEE Trans. Power Electron.* **2023**, *38*, 11352–11367. [[CrossRef](#)]
53. Kashif, M.; Singh, B. Modified Active-Power MRAS Based Adaptive Control With Reduced Sensors for PMSM Operated Solar Water Pump. *IEEE Trans. Energy Convers.* **2023**, *38*, 38–52. [[CrossRef](#)]
54. Sun, X.; Li, T.; Yao, M.; Lei, G.; Guo, Y.; Zhu, J. Improved finite-control-set model predictive control with virtual vectors for PMSM drives. *IEEE Trans. Energy Convers.* **2022**, *37*, 1885–1894. [[CrossRef](#)]
55. Kivanc, O.C.; Ozturk, S.B. Sensorless PMSM Drive Based on Stator Feedforward Voltage Estimation Improved With MRAS Multiparameter Estimation. *IEEE/ASME Trans. Mechatron.* **2018**, *23*, 1326–1337. [[CrossRef](#)]

56. Badini, S.S.; Verma, V. A New Stator Resistance Estimation Technique for Vector-Controlled PMSM Drive. *IEEE Trans. Ind. Appl.* **2020**, *56*, 6536–6545. [[CrossRef](#)]
57. Kim, H.-W.; Youn, M.-J.; Cho, K.-Y. New voltage distortion observer of PWM VSI for PMSM. *IEEE Trans. Ind. Electron.* **2005**, *52*, 1188–1192. [[CrossRef](#)]
58. Sun, X.; Zhang, Y.; Tian, X.; Cao, J.; Zhu, J. Speed Sensorless Control for IPMSMs Using a Modified MRAS With Gray Wolf Optimization Algorithm. *IEEE Trans. Transp. Electr.* **2022**, *8*, 1326–1337. [[CrossRef](#)]
59. Liu, Z.-H.; Nie, J.; Wei, H.-L.; Chen, L.; Li, X.-H.; Zhang, H.-Q. A Newly Designed VSC-Based Current Regulator for Sensorless Control of PMSM Considering VSI Nonlinearity. *IEEE J. Emerg. Sel. Top. Power Electron.* **2021**, *9*, 4420–4431. [[CrossRef](#)]
60. Chen, D.; Wang, J.; Zhou, L. Adaptive Second-Order Active-Flux Observer for Sensorless Control of PMSMs With MRAS-Based VSI Nonlinearity Compensation. *IEEE J. Emerg. Sel. Top. Power Electron.* **2023**, *11*, 3076–3086. [[CrossRef](#)]
61. Liu, Z.-H.; Nie, J.; Wei, H.-L.; Chen, L.; Wu, F.-M.; Lv, M.-Y. Second-Order ESO-Based Current Sensor Fault-Tolerant Strategy for Sensorless Control of PMSM With B-Phase Current. *IEEE/ASME Trans. Mechatron.* **2022**, *27*, 5427–5438. [[CrossRef](#)]
62. Chen, D.; Li, J.; Chen, J.; Qu, R. On-Line Compensation of Resolver Periodic Error for PMSM Drives. *IEEE Trans. Ind. Appl.* **2019**, *55*, 5990–6000. [[CrossRef](#)]
63. Zhu, Y.; Cheng, M.; Hua, W.; Zhang, B. Sensorless Control Strategy of Electrical Variable Transmission Machines for Wind Energy Conversion Systems. *IEEE Trans. Magn.* **2013**, *49*, 3383–3386. [[CrossRef](#)]
64. Kim, H.-W.; Youn, M.-J.; Cho, K.-Y.; Kim, H.-S. Nonlinearity estimation and compensation of PWM VSI for PMSM under resistance and flux linkage uncertainty. *IEEE Trans. Control. Syst. Technol.* **2006**, *14*, 589–601.
65. Jin, Z.; Yang, J.; Qiu, X.; Ge, H.; Bai, C. A High Torque Estimation Accuracy Direct Torque Control of Permanent Magnet Synchronous Motor Based on a Novel Iron Loss Resistance Observer. *IEEE Access* **2021**, *9*, 125822–125829. [[CrossRef](#)]
66. Sun, X.; Zhu, Y.; Cai, Y.; Xiong, Y.; Yao, M.; Yuan, C. Current fault tolerance control strategy for 3-phase switched reluctance motor combined with position signal reconstruction. *IEEE Trans. Energy Convers.* **2023**. [[CrossRef](#)]
67. Bolognani, S.; Oboe, R.; Zigliotto, M. Sensorless full-digital PMSM drive with EKF estimation of speed and rotor position. *IEEE Trans. Ind. Electron.* **1999**, *46*, 184–191. [[CrossRef](#)]
68. Wang, Z.; Zheng, Y.; Zou, Z.; Cheng, M. Position Sensorless Control of Interleaved CSI Fed PMSM Drive With Extended Kalman Filter. *IEEE Trans. Magn.* **2012**, *48*, 3688–3691. [[CrossRef](#)]
69. Yang, H.; Yang, R.; Hu, W.; Huang, Z. FPGA-Based Sensorless Speed Control of PMSM Using Enhanced Performance Controller Based on the Reduced-Order EKF. *IEEE J. Emerg. Sel. Top. Power Electron.* **2021**, *9*, 289–301. [[CrossRef](#)]
70. Xiao, X.; Chen, C. Reduction of Torque Ripple Due to Demagnetization in PMSM Using Current Compensation. *IEEE Trans. Appl. Supercond.* **2010**, *20*, 1068–1071. [[CrossRef](#)]
71. Sun, X.; Tang, X.; Tian, X.; Wu, J.; Zhu, J. Position sensorless control of switched reluctance motor drives based on a new sliding mode observer using Fourier flux linkage model. *IEEE Trans. Energy Convers.* **2022**, *37*, 978–988. [[CrossRef](#)]
72. Zwerger, T.; Mercorelli, P. Using a Bivariate Polynomial in an EKF for State and Inductance Estimations in the Presence of Saturation Effects to Adaptively Control a PMSM. *IEEE Access* **2022**, *10*, 111545–111553. [[CrossRef](#)]
73. Quang, N.K.; Hieu, N.T.; Ha, Q.P. FPGA-Based Sensorless PMSM Speed Control Using Reduced-Order Extended Kalman Filters. *IEEE Trans. Ind. Electron.* **2014**, *61*, 6574–6582. [[CrossRef](#)]
74. Sun, X.; Cao, J.; Lei, G.; Guo, Y.; Zhu, J. A Composite Sliding Mode Control for SPMSM Drives Based on a New Hybrid Reaching Law With Disturbance Compensation. *IEEE Trans. Transp. Electr.* **2021**, *7*, 1427–1436. [[CrossRef](#)]
75. Yang, Z.; Yan, Z.; Lu, Y.; Wang, W.; Yu, L.; Geng, Y. Double DOF Strategy for Continuous-Wave Pulse Generator Based on Extended Kalman Filter and Adaptive Linear Active Disturbance Rejection Control. *IEEE Trans. Power Electron.* **2022**, *37*, 1382–1393. [[CrossRef](#)]
76. Bolognani, S.; Tubiana, L.; Zigliotto, M. Extended Kalman filter tuning in sensorless PMSM drives. *IEEE Trans. Ind. Appl.* **2003**, *39*, 1741–1747. [[CrossRef](#)]
77. Li, X.; Kennel, R. General Formulation of Kalman-Filter-Based Online Parameter Identification Methods for VSI-Fed PMSM. *IEEE Trans. Ind. Electron.* **2021**, *68*, 2856–2864. [[CrossRef](#)]
78. Xiao, X.; Chen, C.; Zhang, M. Dynamic Permanent Magnet Flux Estimation of Permanent Magnet Synchronous Machines. *IEEE Trans. Appl. Supercond.* **2010**, *20*, 1085–1088. [[CrossRef](#)]
79. Li, X.; Zhang, S.; Cui, X.; Wang, Y.; Zhang, C.; Li, Z.; Zhou, Y. Novel Deadbeat Predictive Current Control for PMSM With Parameter Updating Scheme. *IEEE J. Emerg. Sel. Top. Power Electron.* **2022**, *10*, 2065–2074. [[CrossRef](#)]
80. Mwasilu, F.; Jung, J.-W. Enhanced Fault-Tolerant Control of Interior PMSMs Based on an Adaptive EKF for EV Traction Applications. *IEEE Trans. Power Electron.* **2016**, *31*, 5746–5758. [[CrossRef](#)]
81. Diao, S.; Diallo, D.; Makni, Z.; Marchand, C.; Bisson, J.-F. A Differential Algebraic Estimator for Sensorless Permanent-Magnet Synchronous Machine Drive. *IEEE Trans. Energy Convers.* **2015**, *30*, 82–89. [[CrossRef](#)]
82. Li, W.; Feng, G.; Li, Z.; Toulabi, M.S.; Kar, N.C. Extended Kalman Filter Based Inductance Estimation for Dual Three-Phase Permanent Magnet Synchronous Motors Under the Single Open-Phase Fault. *IEEE Trans. Energy Convers.* **2022**, *37*, 1134–1144. [[CrossRef](#)]
83. Smidl, V.; Peroutka, Z. Advantages of Square-Root Extended Kalman Filter for Sensorless Control of AC Drives. *IEEE Trans. Ind. Electron.* **2012**, *59*, 4189–4196. [[CrossRef](#)]

84. Sun, X.; Tang, X.; Tian, X.; Lei, G.; Guo, Y.; Zhu, J. Sensorless control with fault-tolerant ability for switched reluctance motors. *IEEE Trans. Energy Convers.* **2022**, *37*, 1272–1281. [[CrossRef](#)]
85. Zuo, S.; Hu, X.; Li, D.; Mao, Y.; Wu, Z.; Xiong, Y. Analysis and Suppression of Longitudinal Vibration of Electric Wheel System Considering Rotor Position Error. *IEEE Trans. Transp. Electrif.* **2021**, *7*, 671–682. [[CrossRef](#)]
86. Wu, Q.; Dong, S.; Zhang, W.-A.; Yu, L. Online Modeling of the CNC Engraving System With Dead-Zone Input Nonlinearity. *IEEE Trans. Ind. Electron.* **2022**, *69*, 774–782. [[CrossRef](#)]
87. Shi, Z.; Sun, X.; Cai, Y.; Yang, Z. Robust Design Optimization of a Five-Phase PM Hub Motor for Fault-Tolerant Operation Based on Taguchi Method. *IEEE Trans. Energy Convers.* **2020**, *35*, 2036–2044. [[CrossRef](#)]
88. Yang, J.; Zhou, J.; Zhou, H.; Yi, F.; Song, D.; Dong, M. High-Precision Harmonic Current Extraction for PMSM Based on Multiple Reference Frames Considering Speed Harmonics. *IEEE Trans. Ind. Electron.* **2023**, *70*, 9764–9776. [[CrossRef](#)]
89. Li, Z.; Feng, G.; Lai, C.; Banerjee, D.; Li, W.; Kar, N.C. Current Injection-Based Multi-parameter Estimation for Dual Three-Phase IPMSM Considering VSI Nonlinearity. *IEEE Trans. Transp. Electrif.* **2019**, *5*, 405–415. [[CrossRef](#)]
90. Brosch, A.; Wallscheid, O.; Böcker, J. Long-Term Memory Recursive Least Squares Online Identification of Highly Utilized Permanent Magnet Synchronous Motors for Finite-Control-Set Model Predictive Control. *IEEE Trans. Power Electron.* **2023**, *38*, 1451–1467. [[CrossRef](#)]
91. Zhou, Y.; Zhang, S.; Cui, X.; Zhang, C.; Li, X. An Accurate Torque Output Method for Open-End Winding Permanent Magnet Synchronous Motors Drives. *IEEE Trans. Energy Convers.* **2021**, *36*, 3470–3480. [[CrossRef](#)]
92. Sun, X.; Wu, M.; Yin, C.; Wang, S. Model Predictive Thrust Force Control for Linear Motor Actuator used in Active Suspension. *IEEE Trans. Energy Convers.* **2021**, *36*, 3063–3072. [[CrossRef](#)]
93. Sun, X.; Cao, J.; Lei, G.; Guo, Y.; Zhu, J. Speed sensorless control for permanent magnet synchronous motors based on finite position set. *IEEE Trans. Ind. Electron.* **2020**, *67*, 6089–6100. [[CrossRef](#)]
94. Yu, Y.; Huang, X.; Li, Z.; Wu, M.; Shi, T.; Cao, Y.; Yang, G.; Niu, F. Full Parameter Estimation for Permanent Magnet Synchronous Motors. *IEEE Trans. Ind. Electron.* **2023**, *69*, 4376–4386. [[CrossRef](#)]
95. Song, J.; Wang, Y.-K.; Zheng, W.X.; Niu, Y. Adaptive Terminal Sliding Mode Speed Regulation for PMSM Under Neural-Network-Based Disturbance Estimation: A Dynamic-Event-Triggered Approach. *IEEE Trans. Ind. Electron.* **2023**, *70*, 8446–8456. [[CrossRef](#)]
96. Liu, Z.L.H.W.X.L.K.; Zhong, Q. Global identification of electrical and mechanical parameters in PMSM drive based on dynamic self-learning PSO. *IEEE Trans. Power Electron.* **2018**, *33*, 10858–10871. [[CrossRef](#)]
97. Sun, X.; Wu, M.; Lei, G.; Guo, Y.; Zhu, J. An improved model predictive current control for PMSM drives based on current track circle. *IEEE Trans. Ind. Electron.* **2021**, *68*, 3782–3793. [[CrossRef](#)]
98. Xiao, Z.L.H.W.Q.Z.K.L.X.; Wu, L. GPU implementation of DPSSO-RE algorithm for parameters identification of surface PMSM considering VSI nonlinearity. *IEEE Trans. Emerg. Sel. Topics Power Electron.* **2017**, *5*, 1334–1345.
99. Sun, X.; Shi, Z.; Lei, G.; Guo, Y.; Zhu, J. Multi-objective design optimization of an IPMSM based on multilevel strategy. *IEEE Trans. Ind. Electron.* **2021**, *68*, 139–148. [[CrossRef](#)]
100. Wang, Y.; Feng, Y.; Zhang, X.; Liang, J. A New Reaching Law for Antidisturbance Sliding-Mode Control of PMSM Speed Regulation System. *IEEE Trans. Power Electron.* **2020**, *35*, 4117–4126. [[CrossRef](#)]
101. Liu, C.; Shang, J. Sensorless Drive Strategy of Open-End Winding PMSM With Zero-Sequence Current Suppression. *IEEE Trans. Energy Convers.* **2021**, *36*, 2987–2997. [[CrossRef](#)]
102. Chen, S.; Ding, W.; Hu, R.; Wu, X.; Shi, S. Sensorless Control of PMSM Drives Using Reduced Order Quasi Resonant-Based ESO and Newton–Raphson Method-Based PLL. *IEEE Trans. Power Electron.* **2023**, *38*, 229–244. [[CrossRef](#)]
103. Zhang, M.; Xia, B.; Zhang, J. Parameter Design and Convergence Analysis of Flux Observer for Sensorless PMSM Drives. *IEEE Trans. Energy Convers.* **2022**, *37*, 2512–2524. [[CrossRef](#)]
104. Sun, X.; Zhang, Y.; Lei, G.; Guo, Y.; Zhu, J. An improved deadbeat predictive stator flux control with reduced-order disturbance observer for in-wheel PMSMs. *IEEE/ASME Trans. Mechatron.* **2021**, *27*, 690–700. [[CrossRef](#)]
105. Qu, L.; Qiao, W.; Qu, L. An Extended-State-Observer-Based Sliding-Mode Speed Control for Permanent-Magnet Synchronous Motors. *IEEE J. Emerg. Sel. Top. Power Electron.* **2021**, *9*, 1605–1613. [[CrossRef](#)]
106. Filho, C.J.V.; Vieira, R.P. Adaptive Full-Order Observer Analysis and Design for Sensorless Interior Permanent Magnet Synchronous Motors Drives. *IEEE Trans. Ind. Electron.* **2021**, *68*, 6527–6536. [[CrossRef](#)]
107. Sun, X.; Zhang, Y.; Cai, Y.; Tian, X. Compensated deadbeat predictive current control considering disturbance and VSI nonlinearity for in-wheel PMSMs. *IEEE/ASME Trans. Mechatron.* **2022**, *27*, 3536–3547. [[CrossRef](#)]
108. Liu, H.; Li, S. Speed Control for PMSM Servo System Using Predictive Functional Control and Extended State Observer. *IEEE Trans. Ind. Electron.* **2012**, *59*, 1171–1183. [[CrossRef](#)]
109. Filho, C.J.V.; Scalcon, F.P.; Gabbi, T.S.; Vieira, R.P. Adaptive observer for sensorless permanent magnet synchronous machines with online pole placement. In Proceedings of the 2017 Brazilian Power Electronics Conference (COBEP), Juiz de Fora, Brazil, 19–22 November 2017; pp. 1–6.
110. Sun, X.; Shi, Z.; Cai, Y.; Lei, G.; Guo, Y.; Zhu, J. Driving-cycle oriented design optimization of a permanent magnet hub motor drive system for a four-wheel-drive electric vehicle. *IEEE Trans. Transp. Electrif.* **2020**, *6*, 1115–1125. [[CrossRef](#)]
111. Yang, M.; Lang, X.; Long, J.; Xu, D. Flux Immunity Robust Predictive Current Control With Incremental Model and Extended State Observer for PMSM Drive. *IEEE Trans. Power Electron.* **2017**, *32*, 9267–9279.

112. Xie, G.; Lu, K.; Dwivedi, S.K.; Rosholm, J.R.; Blaabjerg, F. Minimum-Voltage Vector Injection Method for Sensorless Control of PMSM for Low-Speed Operations. *IEEE Trans. Power Electron.* **2016**, *31*, 1785–1794. [[CrossRef](#)]
113. Wen, D.; Wang, W.; Zhang, Y. Sensorless Control of Permanent Magnet Synchronous Motor in Full Speed Range. *Chin. J. Electr. Eng.* **2022**, *8*, 97–107. [[CrossRef](#)]
114. Song, X.; Han, B.; Zheng, S.; Chen, S. A Novel Sensorless Rotor Position Detection Method for High-Speed Surface PM Motors in a Wide Speed Range. *IEEE Trans. Power Electron.* **2018**, *33*, 7083–7093. [[CrossRef](#)]
115. Wu, C.; Zhao, Y.; Sun, M. Enhancing Low-Speed Sensorless Control of PMSM Using Phase Voltage Measurements and Online Multiple Parameter Identification. *IEEE Trans. Power Electron.* **2020**, *35*, 10700–10710. [[CrossRef](#)]
116. Lin, H.; Liao, Y.; Yan, L.; Li, F.; Feng, Y. A Novel Modulation-Based Current Harmonic Control Strategy for PMSM Considering Current Measurement Error and Asymmetric Impedance. *IEEE Access* **2022**, *10*, 89346–89357.
117. Sun, X.; Hu, C.; Lei, G.; Yang, Z.; Guo, Y.; Zhu, J. Speed sensorless control of SPMSM drives for EVs with a binary search algorithm-based phase-locked loop. *IEEE Trans. Veh. Technol.* **2020**, *69*, 4968–4978.
118. Song, S.I.K.J.H.I.E.Y.; Kim, R.Y. A new rotor position estimation method of IPMSM using all-pass filter on high-frequency rotating voltage signal injection. *IEEE Trans. Ind. Electron.* **2016**, *63*, 6499–6509.
119. Shinnaka, R.H.S.; Nakamura, N. New sensorless vector control of PMSM by discrete-time voltage injection of PWM carrier frequency-sine- and cosine-form amplitudes extraction method. In Proceedings of the IECON 2016—42nd Annual Conference of the IEEE Industrial Electronics Society, Florence, Italy, 23–26 October 2016; pp. 2862–2867.
120. Dietrich, L.C.G.G.S.; Hahn, I. Self-sensing control of permanent-magnet synchronous machines with multiple saliencies using pulse-voltage-injection. *IEEE Trans. Ind. Appl.* **2016**, *52*, 3480–3491.
121. Jin, Z.; Sun, X.; Lei, G.; Guo, Y.; Zhu, J. Sliding mode direct torque control of SPMSMs based on a hybrid wolf optimization algorithm. *IEEE Trans. Ind. Electron.* **2022**, *69*, 4534–4544. [[CrossRef](#)]
122. Corley, M.J.; Lorenz, R.D. Rotor position and velocity estimation for a salient-pole permanent magnet synchronous machine at standstill and high speeds. *IEEE Trans. Ind. Appl.* **1998**, *34*, 784–789. [[CrossRef](#)]
123. Medjmadj, S.; Diallo, D.; Mostefai, M.; Delpha, C.; Arias, A. PMSM drive position estimation: Contribution to the high-frequency injection voltage selection issue. *IEEE Trans. Energy Convers.* **2015**, *30*, 349–358.
124. Harke, D.R.M.C.; Lorenz, R.D. Robust magnet polarity estimation for initialization of PM synchronous machines with near-zero saliency. *IEEE Trans. Ind. Appl.* **2008**, *44*, 1199–1209.
125. Li, T.; Sun, X.; Lei, G.; Yang, Z.; Guo, Y.; Zhu, J. Finite-control-set model predictive control of permanent magnet synchronous motor drive systems—An overview. *IEEE/CAA J. Autom. Sinica* **2022**, *9*, 2087–2105.
126. Xu, P.L.; Zhu, Z.Q. Novel square-wave signal injection method using zero-sequence voltage for sensorless control of PMSM drives. *IEEE Trans. Ind. Electron.* **2016**, *63*, 7444–7454. [[CrossRef](#)]
127. Xu, P.L.; Zhu, Z.Q. Novel carrier signal injection method using zero-sequence voltage for sensorless control of PMSM drives. *IEEE Trans. Ind. Electron.* **2016**, *63*, 2053–2061.
128. Luo, X.; Tang, Q.; Shen, A.; Zhang, Q. PMSM Sensorless Control by Injecting HF Pulsating Carrier Signal Into Estimated Fixed-Frequency Rotating Reference Frame. *IEEE Trans. Ind. Electron.* **2016**, *63*, 2294–2303.
129. Zhang, X.; Li, H.; Yang, S.; Ma, M. Improved Initial Rotor Position Estimation for PMSM Drives Based on HF Pulsating Voltage Signal Injection. *IEEE Trans. Ind. Electron.* **2018**, *65*, 4702–4713.
130. Almarhoon, A.H.; Zhu, Z.Q.; Xu, P.L. Improved Pulsating Signal Injection Using Zero-Sequence Carrier Voltage for Sensorless Control of Dual Three-Phase PMSM. *IEEE Trans. Energy Convers.* **2017**, *32*, 436–446. [[CrossRef](#)]
131. Tang, Q.; Shen, A.; Luo, X.; Xu, J. PMSM Sensorless Control by Injecting HF Pulsating Carrier Signal Into ABC Frame. *IEEE Trans. Power Electron.* **2017**, *32*, 3767–3776. [[CrossRef](#)]
132. Liu, J.M.; Zhu, Z.Q. Novel Sensorless Control Strategy With Injection of High-Frequency Pulsating Carrier Signal Into Stationary Reference Frame. *IEEE Trans. Ind. Appl.* **2014**, *50*, 2574–2583.
133. Xu, Z.; Zhang, J.; Cheng, M. Investigation of Signal Injection Methods for Fault Detection of PMSM Drives. *IEEE Trans. Energy Convers.* **2022**, *37*, 2207–2216.
134. Mai, Z.; Xiao, F.; Fu, K.; Liu, J.; Lian, C.; Li, K.; Zhang, W. HF Pulsating Carrier Voltage Injection Method Based on Improved Position Error Signal Extraction Strategy for PMSM Position Sensorless Control. *IEEE Trans. Power Electron.* **2021**, *36*, 9348–9360.
135. Xu, P.L.; Zhu, Z.Q. Carrier Signal Injection-Based Sensorless Control for Permanent-Magnet Synchronous Machine Drives Considering Machine Parameter Asymmetry. *IEEE Trans. Ind. Electron.* **2016**, *63*, 2813–2824.
136. Laborda, D.F.; Reigosa, D.D.; Fernández, D.; Sasaki, K.; Kato, T.; Briz, F. Enhanced Torque Estimation in Variable Leakage Flux PMSM Combining High and Low Frequency Signal Injection. *IEEE Trans. Ind. Appl.* **2023**, *59*, 801–813.
137. Reigosa, D.D.; Fernandez, D.; Yoshida, H.; Kato, T.; Briz, F. Permanent-Magnet Temperature Estimation in PMSMs Using Pulsating High-Frequency Current Injection. *IEEE Trans. Ind. Appl.* **2015**, *51*, 3159–3168. [[CrossRef](#)]
138. Basic, D.; Malrait, F.; Rouchon, P. Current Controller for Low-Frequency Signal Injection and Rotor Flux Position Tracking at Low Speeds. *IEEE Trans. Ind. Electron.* **2011**, *58*, 4010–4022. [[CrossRef](#)]
139. Wang, S.; Yang, K.; Chen, K. An Improved Position-Sensorless Control Method at Low Speed for PMSM Based on High-Frequency Signal Injection into a Rotating Reference Frame. *IEEE Access* **2019**, *7*, 86510–86521. [[CrossRef](#)]
140. Reigosa, D.D.; Fernandez, D.; Tanimoto, T.; Kato, T.; Briz, F. Sensitivity Analysis of High-Frequency Signal Injection-Based Temperature Estimation Methods to Machine Assembling Tolerances. *IEEE Trans. Ind. Appl.* **2016**, *52*, 4798–4805.

141. Reigosa, D.; Fernandez, D.; Tanimoto, T.; Kato, T.; Briz, F. Comparative Analysis of BEMF and Pulsating High-Frequency Current Injection Methods for PM Temperature Estimation in PMSMs. *IEEE Trans. Power Electron.* **2017**, *32*, 3691–3699.
142. Accetta, A.; Cirrincione, M.; Pucci, M.; Vitale, G. Sensorless Control of PMSM Fractional Horsepower Drives by Signal Injection and Neural Adaptive-Band Filtering. *IEEE Trans. Ind. Electron.* **2012**, *59*, 1355–1366. [[CrossRef](#)]
143. Lara, J.; Chandra, A. Performance Investigation of Two Novel HFSI Demodulation Algorithms for Encoderless FOC of PMSMs Intended for EV Propulsion. *IEEE Trans. Ind. Electron.* **2018**, *65*, 1074–1083. [[CrossRef](#)]
144. Jin, X.; Ni, R.; Chen, W.; Blaabjerg, F.; Xu, D. High-Frequency Voltage-Injection Methods and Observer Design for Initial Position Detection of Permanent Magnet Synchronous Machines. *IEEE Trans. Power Electron.* **2018**, *33*, 7971–7979. [[CrossRef](#)]
145. Raca, D.; Garcia, P.; Reigosa, D.D.; Briz, F.; Lorenz, R.D. Carrier-Signal Selection for Sensorless Control of PM Synchronous Machines at Zero and Very Low Speeds. *IEEE Trans. Ind. Appl.* **2010**, *46*, 167–178. [[CrossRef](#)]
146. Fu, X.; Xu, Y.; He, H.; Fu, X. Initial Rotor Position Estimation by Detecting Vibration of Permanent Magnet Synchronous Machine. *IEEE Trans. Ind. Electron.* **2021**, *68*, 6595–6606. [[CrossRef](#)]
147. Wang, Z.; Cao, Z.; He, Z. Improved Fast Method of Initial Rotor Position Estimation for Interior Permanent Magnet Synchronous Motor by Symmetric Pulse Voltage Injection. *IEEE Access* **2020**, *8*, 59998–60007. [[CrossRef](#)]
148. Zhang, G.; Wang, G.; Wang, H.; Xiao, D.; Li, L.; Xu, D. Pseudo-random-frequency sinusoidal injection-based sensorless IPMSM drives with tolerance for system delays. *IEEE Trans. Power Electron.* **2019**, *34*, 3623–3632. [[CrossRef](#)]
149. Murakami, S.; Shiota, T.; Ohto, M.; Ide, K.; Hisatsune, M. Encoderless servo drive with adequately designed IPMSM for pulse-voltage-injection-based position detection. *IEEE Trans. Ind. Appl.* **2012**, *48*, 1922–1930. [[CrossRef](#)]
150. Wang, G.; Zhou, H.; Zhao, N.; Li, C.; Xu, D. Sensorless control of IPMSM drives using a pseudo-random phase-switching fixed-frequency signal injection scheme. *IEEE Trans. Ind. Electron.* **2018**, *65*, 7660–7671. [[CrossRef](#)]
151. Wang, G.; Zhou, H.; Zhao, N.; Li, C.; Xu, D. Sensorless control scheme of IPMSMs using HF orthogonal square-wave voltage injection into a stationary reference frame. *IEEE Trans. Power Electron.* **2019**, *34*, 2573–2584. [[CrossRef](#)]
152. Li, C.; Wang, G.; Zhang, G.; Xu, D.; Xiao, D. Saliency-based sensorless control for SynRM drives with suppression of position estimation error. *IEEE Trans. Ind. Electron.* **2019**, *66*, 5839–5849. [[CrossRef](#)]
153. Yang, S.C.; Yang, S.M.; Hu, J.H. Design consideration on the square-wave voltage injection for sensorless drive of interior permanent-magnet machines. *IEEE Trans. Ind. Electron.* **2017**, *64*, 159–168. [[CrossRef](#)]
154. Wang, G.; Yang, L.; Zhang, G.; Zhang, X.; Xu, D. Comparative investigation of pseudorandom high-frequency signal injection schemes for sensorless IPMSM drives. *IEEE Trans. Power Electron.* **2017**, *32*, 2123–2132. [[CrossRef](#)]
155. Wang, G.; Xiao, D.; Zhao, N.; Zhang, X.; Wang, W.; Xu, D. Low-frequency pulse voltage injection scheme-based sensorless control of IPMSM drives for audible noise reduction. *IEEE Trans. Ind. Electron.* **2017**, *64*, 8415–8426. [[CrossRef](#)]
156. Ni, R.; Xu, D.; Blaabjerg, F.; Lu, K.; Wang, G.; Zhang, G. Square-wave voltage injection algorithm for PMSM position sensorless control with high robustness to voltage errors. *IEEE Trans. Power Electron.* **2017**, *32*, 5425–5437. [[CrossRef](#)]
157. Kim, D.; Kwon, Y.C.; Sul, S.K.; Kim, J.H.; Yu, R.S. Suppression of injection voltage disturbance for high-frequency square-wave injection sensorless drive with regulation of induced high-frequency current ripple. *IEEE Trans. Ind. Appl.* **2016**, *52*, 302–312. [[CrossRef](#)]
158. Demmelmayr, F.; Troyer, M.; Schroedl, M. Advantages of PM-machines compared to induction machines in terms of efficiency and sensorless control in traction applications. In Proceedings of the IECON 2011—37th Annual Conference of the IEEE Industrial Electronics Society, Melbourne, VIC, Australia, 7–10 November 2011; pp. 2762–2768.
159. Hofer, M.; Nikowitz, M.; Schroedl, M. Sensorless control of a reluctance synchronous machine in the whole speed range without voltage pulse injections. In Proceedings of the 2017 IEEE 3rd International Future Energy Electronics Conference and ECCE Asia (IFECC 2017—ECCE Asia), Kaohsiung, Taiwan, 3–7 June 2017; pp. 1194–1198.
160. Robeischl, E.; Schroedl, M. Optimized inform measurement sequence for sensorless PM synchronous motor drives with respect to minimum current distortion. *IEEE Trans. Ind. Appl.* **2004**, *40*, 591–598. [[CrossRef](#)]
161. Zhao, C.; Tanaskovic, M.; Percacci, F.; Mariéthoz, S.; Gnos, P. Sensorless position estimation for slotless surface mounted permanent magnet synchronous motors in full speed range. *IEEE Trans. Power Electron.* **2019**, *34*, 11566–11579. [[CrossRef](#)]
162. Hind, D.; Li, C.; Sumner, M.; Gerada, C. Realising robust low speed sensorless PMSM control using current derivatives obtained from standard current sensors. In Proceedings of the 2017 IEEE International Electric Machines and Drives Conference (IEMDC), Miami, FL, USA, 21–24 May 2017; pp. 1–6.
163. Guan, D.Q.; Bui, M.X.; Xiao, D.; Rahman, M.F. Performance comparison of two FPE sensorless control methods on a direct torque controlled interior permanent magnet synchronous motor drive. In Proceedings of the 2016 19th International Conference on Electrical Machines and Systems (ICEMS), Chiba, Japan, 13–16 November 2016; pp. 1–6.
164. Wang, G.; Kuang, J.; Zhao, N.; Zhang, G.; Xu, D. Rotor position estimation of PMSM in low-speed region and standstill using zero-voltage vector injection. *IEEE Trans. Power Electron.* **2018**, *33*, 7948–7958. [[CrossRef](#)]
165. Xie, G.; Lu, K.; Dwivedi, S.K.; Riber, R.J.; Wu, W. Permanent magnet flux online estimation based on zero-voltage vector injection method. *IEEE Trans. Power Electron.* **2015**, *30*, 6506–6509. [[CrossRef](#)]
166. Guan, D.Q.; Bui, M.X.; Xiao, D.; Rahman, M.F. Evaluation of an FPGA current derivative measurement system for the fundamental PWM excitation sensorless method for IPMSM. In Proceedings of the 2016 IEEE 2nd Annual Southern Power Electronics Conference (SPEC), Auckland, New Zealand, 5–8 December 2016; pp. 1–6.

167. Xie, G.; Lu, K.; Kumar, D.S.; Riber, R.J. High bandwidth zero voltage injection method for sensorless control of PMSM. In Proceedings of the 2014 17th International Conference on Electrical Machines and Systems (ICEMS), Hangzhou, China, 22–25 October 2014; pp. 3546–3552.
168. Al-Kaf, H.A.G.; Lee, K.-B. Low Complexity MPC-DSVPWM for Current Control of PMSM Using Neural Network Approach. *IEEE Access* **2022**, *10*, 132596–132607. [[CrossRef](#)]
169. Zhang, Z.; Wang, Z.; Wei, X.; Liang, Z.; Kennel, R.; Rodriguez, J. Space-Vector-Optimized Predictive Control for Dual Three-Phase PMSM With Quick Current Response. *IEEE Trans. Power Electron.* **2022**, *37*, 4453–4462.
170. Fuentes, E.; Silva, C.A.; Kennel, R.M. MPC Implementation of a Quasi-Time-Optimal Speed Control for a PMSM Drive, with Inner Modulated-FS-MPC Torque Control. *IEEE Trans. Ind. Electron.* **2016**, *63*, 3897–3905.
171. Lee, Y.; Sul, S.K. Model-based sensorless control of an IPMSM with enhanced robustness against load disturbances based on position and speed estimator using a speed error. *IEEE Trans. Ind. Appl.* **2018**, *54*, 1448–1459.
172. Lin, T.C.; Zhu, Z.Q.; Liu, J.M. Improved rotor position estimation in sensorless-controlled permanent-magnet synchronous machines having asymmetric-EMF with harmonic compensation. *IEEE Trans. Ind. Electron.* **2015**, *62*, 6131–6139.
173. Tuovinen, T.; Hinkkanen, M. Signal-injection-assisted full-order observer with parameter adaptation for synchronous reluctance motor drives. *IEEE Trans. Ind. Appl.* **2014**, *50*, 3392–3402.
174. Bao, D.; Pan, X.; Wang, Y.; Li, K. Adaptive synchronous-frequency tracking-mode observer for the sensorless control of a surface PMSM. *IEEE Trans. Ind. Appl.* **2018**, *54*, 6460–6471.
175. Feng, Y.; Yu, X.; Han, F. High-order terminal sliding-mode observer for parameter estimation of a permanent-magnet synchronous motor. *IEEE Trans. Ind. Electron.* **2013**, *60*, 4272–4280.
176. Foo, G.; Rahman, M.F. Evaluation of velocity servo performance of IPMSM drive under high-performance sensorless operation. In Proceedings of the 8th International Conference on Power Electronics—ECCE Asia, Jeju, Republic of Korea, 30 May–3 June 2011; pp. 1–10.
177. Scarcella, G.; Scelba, G.; Testa, A. High performance sensorless controls based on HF excitation: A viable solution for future AC motor drives? In Proceedings of the 2015 IEEE Workshop on Electrical Machines Design, Control and Diagnosis (WEMDCD), Turin, Italy, 26–27 March 2015; pp. 178–187.
178. Gabriel, F.; De Belie, F.; Neyt, X.; Lataire, P. High-frequency issues using rotating voltage injections intended for position self-sensing. *IEEE Trans. Ind. Electron.* **2013**, *60*, 5447–5457.
179. Zhao, Y.; Qiao, W.; Wu, L. Improved rotor position and speed estimators for sensorless control of interior permanent-magnet synchronous machines. *IEEE J. Emerg. Sel. Topics Power Electron.* **2014**, *2*, 627–639.
180. Sato, S.; Iura, H.; Ide, K.; Sul, S.K. Three years of industrial experience with sensorless IPMSM drive based on high frequency injection method. In Proceedings of the 2011 Symposium on Sensorless Control for Electrical Drives, Birmingham, UK, 1–2 September 2011; pp. 74–79.
181. Chen, Y.; Wang, X.; Meng, X.; He, M.; Xiao, D.; Wang, Z. A Universal Model Predictive Control Strategy for Dual Inverters Fed OW-PMSM Drives. *IEEE Trans. Power Electron.* **2023**, *38*, 7575–7585.
182. Friedmann, J.; Hoffmann, R.; Kennel, R. A new approach for a complete and ultrafast analysis of PMSMs using the arbitrary injection scheme. In Proceedings of the 2016 IEEE Symposium on Sensorless Control for Electrical Drives (SLED), Nadi, Fiji, 5–6 June 2016; pp. 1–6.
183. Shi, Z.; Sun, X.; Cai, Y.; Yang, Z.; Lei, G.; Guo, Y.; Zhu, J. Torque analysis and dynamic performance improvement of A PMSM for EVs by skew angle optimization. *IEEE Trans. Appl. Supercon.* **2019**, *29*, 0600305.
184. Hosogaya, Y.; Kubota, H. Flux position estimation method of IPMSM by controlling current derivative at zero voltage vector. In Proceedings of the 2010 International Conference on Electrical Machines and Systems, Incheon, Republic of Korea, 10–13 October 2010; pp. 894–899.
185. Sun, X.; Cao, Y.; Jin, Z.; Tian, X.; Xue, M. An adaptive ECMS based on traffic information for plug-in hybrid electric buses. *IEEE Trans. Ind. Electron.* **2023**, *70*, 9248–9259.
186. Shi, Z.; Sun, X.; Lei, G.; Tian, X.; Guo, Y.; Zhu, J. Multiobjective optimization of a five-phase bearingless permanent magnet motor considering winding area. *IEEE/ASME Trans. Mechatron.* **2022**, *27*, 2657–2666.
187. Bolognani, S.; Ortombina, L.; Tinazzi, F.; Zigliotto, M. Model sensitivity of fundamental-frequency-based position estimators for sensorless PM and reluctance synchronous motor drives. *IEEE Trans. Ind. Electron.* **2018**, *65*, 77–85.
188. Sun, X.; Xu, N.; Yao, M. Sequential subspace optimization design of a dual three-phase permanent magnet synchronous hub motor based on NSGA III. *IEEE Trans. Transp. Electr.* **2023**, *9*, 622–630.
189. Yao, C.; Sun, Z.; Xu, S.; Zhang, H.; Ren, G.; Ma, G. ANN Optimization of Weighting Factors Using Genetic Algorithm for Model Predictive Control of PMSM Drives. *IEEE Trans. Ind. Appl.* **2022**, *58*, 7346–7362.
190. Andreescu, G.-D.; Pitic, C.I.; Blaabjerg, F.; Boldea, I. Combined Flux Observer With Signal Injection Enhancement for Wide Speed Range Sensorless Direct Torque Control of IPMSM Drives. *IEEE Trans. Energy Convers.* **2008**, *23*, 393–402.
191. Wang, G.; Yang, R.; Xu, D. DSP-Based Control of Sensorless IPMSM Drives for Wide-Speed-Range Operation. *IEEE Trans. Ind. Electron.* **2013**, *60*, 720–727.
192. Seilmeier, M.; Piepenbreier, B. Sensorless Control of PMSM for the Whole Speed Range Using Two-Degree-of-Freedom Current Control and HF Test Current Injection for Low-Speed Range. *IEEE Trans. Power Electron.* **2015**, *30*, 4394–4403.

193. Hong, D.-K.; Woo, B.-C.; Lee, J.-Y.; Koo, D.-H. Ultra High Speed Motor Supported by Air Foil Bearings for Air Blower Cooling Fuel Cells. *IEEE Trans. Magn.* **2012**, *48*, 871–874.
194. Zhao, L.; Ham, C.; Zheng, L.; Wu, T.; Sundaram, K.; Kapat, J.; Chow, L. A Highly Efficient 200 000 RPM Permanent Magnet Motor System. *IEEE Trans. Magn.* **2007**, *43*, 2528–2530.
195. Ahn, J.-H.; Choi, J.-Y.; Park, C.H.; Han, C.; Kim, C.-W.; Yoon, T.-G. Correlation Between Rotor Vibration and Mechanical Stress in Ultra-High-Speed Permanent Magnet Synchronous Motors. *IEEE Trans. Magn.* **2017**, *53*, 1–6.

Disclaimer/Publisher's Note: The statements, opinions and data contained in all publications are solely those of the individual author(s) and contributor(s) and not of MDPI and/or the editor(s). MDPI and/or the editor(s) disclaim responsibility for any injury to people or property resulting from any ideas, methods, instructions or products referred to in the content.